

Dynamically Feasible Deep Reinforcement Learning Policy for Robot Navigation in Dense Mobile Crowds

Utsav Patel, Nithish Kumar, Adarsh Jagan Sathyamoorthy and Dinesh Manocha.

Abstract—We present a novel Deep Reinforcement Learning (DRL) based policy for mobile robot navigation in dynamic environments that computes dynamically feasible and spatially aware robot velocities. Our method addresses two primary issues associated with the Dynamic Window Approach (DWA) and DRL-based navigation policies and solves them by using the benefits of one method to fix the issues of the other. The issues are: 1. DWA not utilizing the time evolution of the environment while choosing velocities from the dynamically feasible velocity set leading to sub-optimal dynamic collision avoidance behaviors, and 2. DRL-based navigation policies computing velocities that often violate the dynamics constraints such as the non-holonomic and acceleration constraints of the robot. Our DRL-based method generates velocities that are dynamically feasible while accounting for the motion of the obstacles in the environment. This is done by embedding the changes in the environment’s state in a novel observation space and a reward function formulation that reinforces spatially aware obstacle avoidance maneuvers. We evaluate our method in realistic 3-D simulation and on a real differential drive robot in challenging indoor scenarios with crowds of varying densities. We make comparisons with traditional and current state-of-the-art collision avoidance methods and observe significant improvements in terms of collision rate, number of dynamics constraint violations and smoothness. We also conduct ablation studies to highlight the advantages and explain the rationale behind our observation space construction, reward structure and network architecture.

I. INTRODUCTION

It is well established that Deep Reinforcement Learning (DRL)-based local planners [1][2][3] can navigate a non-holonomic/differential drive robot through pedestrian rich environments safely. They are effective in capturing and reacting to the evolution of the environment’s state over time, resulting in excellent dynamic obstacle avoidance capabilities. In addition, these methods employ inexpensive perception sensors such as RGB-D cameras and simple 2-D lidars. However, it is not guaranteed that the instantaneous velocities computed by DRL-based methods will be *dynamically feasible*. That is, the computed velocities must obey the non-holonomic and acceleration constraints of the robot, which could otherwise lead to highly non-smooth and jerky trajectories.

Learning to choose smooth, dynamically feasible velocities during navigation happens through a DRL method’s reward function, where such trajectories and other desirable behaviors are rewarded, and collisions and non-desirable behaviors are penalized. However, a fully trained policy could over-prioritize collision avoidance behavior over dynamic feasibility if the penalty for collision is not appropriately balanced with the reward for computing feasible velocities. Therefore, acceleration limits and the non-holonomic constraints of the robot are largely ignored. The policy learning such fundamental constraints is crucial especially when the robot navigates among humans and in dense scenes.

On the other hand, the Dynamic Window Approach

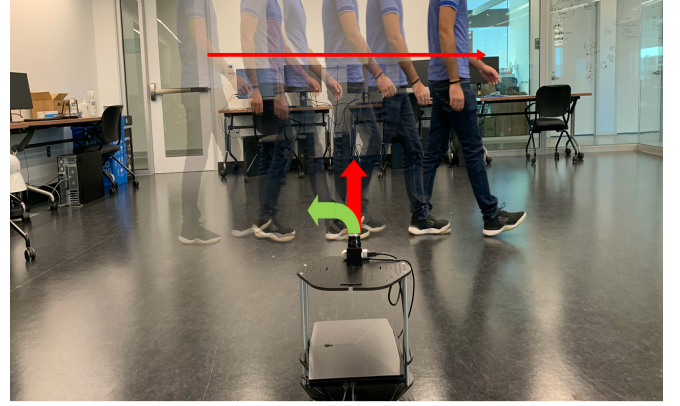


Fig. 1: Our robot handling dynamic obstacles using dynamically feasible, smooth velocities. Our approach considers the motion of the dynamic obstacles while generating the velocities. Our method currently has the least collision rates when compared to DWA [4], CrowdMove, and DenseCAvoid. Since our method samples values from DWA’s velocity space, the robot velocities are guaranteed to be dynamically feasible.

(DWA) [4], a classic navigation algorithm accounts for the robot’s dynamics constraints and guarantees that the velocities in a space known as the *dynamic window* are collision-free and feasible/achievable for the robot within a time horizon Δt . However, DWA’s formulation only considers the robot’s sensor data at the current time instant to make decisions and that limits its performance in highly dynamic environments leading to potentially many collisions.

Our work provides a novel solution to mitigate the limitations of both DRL-based methods and DWA by using the benefit of one to address the shortcoming of the other.

Main Results: We present a DRL-based collision avoidance policy that utilizes a novel observation space formulation and a novel reward function that leads to more spatially aware, collision-free, dynamically feasible velocities for navigation. We show that our approach has a superior performance compared to DWA and DRL methods like Crowdmove [5] and DenseCAvoid [6] in terms of collision rate, smoothness and time to reach the goal satisfying the dynamics constraints of the robot. The main contributions of our work are:

- A novel formulation for the observation space based on the concept of dynamic window is used to train our DRL-based policy. The observation space is constructed by calculating the robot’s feasible velocity set at that time instant and the costs corresponding to using those velocities in the past n time instants. This formulation leads to a significantly lower dimension observation space compared to other DRL methods [2] [6] while also embedding the time evolution of the environment’s

state in the form of costs. This in turn leads to significantly lower training times, and easier sim-to-real transfer of the fully trained policy.

- A novel reward function that is shaped such that the robot’s navigation is more spatially aware. That is, the robot must navigate to a space where the probability of colliding with an obstacle is drastically reduced. This leads to the robot taking swifter trajectories around dynamic obstacles unlike DWA which might directly go in the dynamic obstacle’s way or stops for the obstacles to pass first. This reduces the collision rate by 33%.

II. RELATED WORK

A. Traditional Collision Avoidance in Dynamic Scenes

Global collision avoidance methods [7], [8], [9], [10] provide an optimal trajectory for the entire route, but is generally offline that is not suitable for dynamic obstacles. On the other hand, vector-based local approaches [4] such as DWA use limited sensory information and are computationally efficient to avoid multiple dynamic obstacles. However, such methods can not be globally optimal.

For instance, Curvature-Velocity method [11] solves for obstacle avoidance velocities by formulating it as a constrained optimization problem incorporating goal and vehicle dynamics. It however suffers from local minima issues.

Another instance of such methods is an extended version of DWA [4], which models mobile agents in the environment as cells of an occupancy grid and checks for collision using D* graph search. Collision-free velocities which are then generated using DWA on this grid, work well for linear agents, but not for agents with non-linear trajectories.

DWA* [12] uses look-ahead verification and navigates with high speed and smoothness to avoid local minimas that could arise due to non-convex obstacles. But with limited sensing it is not guaranteed to be effective in every scenario. DW4DOT [13] extends beyond the local window and computes possible paths in the future using a tree approach and is effective for dynamic agents. But it’s working frequency reduces with an increasing number of agents in the environment. In order to deal with environments with multiple dynamic agents DRL-based techniques are a viable option.

B. DRL-based Collision Avoidance

There have been numerous works on DRL-based collision avoidance in recent years. Methods such as [14] have used a deep double-Q network for depth prediction from RGB images for collision avoidance in static environments whereas more advanced methods [15] have exploited Convolutional Neural Networks to model end-to-end visuomotor navigation capabilities.

Obstacle avoidance in previously unseen scenarios filled with pedestrians is demonstrated in [16]. A decentralized, scalable, sensor level collision avoidance proposed in [17] performed better with lesser freezing issues in a new hybrid architecture implemented in [18]. With the assumption that pedestrians’ motions aid in collision avoidance, a cooperative model between robot and pedestrians was proposed in [?]. However, its good performance is limited to sparse crowds. An extension using LSTMs [19] to capture temporal information enabled it to be operational among a larger number of pedestrians.

Symbols	Definitions
k	Number of linear or angular velocities robot can execute at a time instant
n	Number of past time instants used in observation space formulation
v, \dot{v}	Robot’s linear velocity and acceleration
$\omega, \dot{\omega}$	Robot’s angular velocity and acceleration
$dist(v, \omega)$	Function gives the distance to the nearest obstacle from the trajectory generated by velocity vector(v, ω)
v_a, ω_a	Robot’s current linear and angular velocity
$\dot{v}_b, \dot{\omega}_b$	Maximum linear and angular braking deceleration
$\pi_\theta(v^t o^t)$	Policy Network
(p_x, p_y)	Coordinates wrt the odom frame
d_t	Distance between the pedestrian and robot
r	Reward for a specific robot action during training
R^{rob}	Robot’s radius
g	Goal location

TABLE I: List of most used symbols in our work and their definitions.

Another class of works have focused on training policies that make the robot behave in a socially acceptable manner and avoid the well-studied freezing robot problem. For instance, socially acceptable navigation models were developed using simple depth camera images and GAIL (General Adversarial Imitation Learning) in [20]. DenseCAvoid [6] utilized pedestrian prediction models to avoid potential collision spaces and reduces the occurrence of the freezing robot problem. However, the model is still susceptible to oscillations and provides no guarantees on generating dynamically feasible robot velocities.

III. BACKGROUND

In this section we briefly provide details and definitions on the different concepts and components that are used in our work.

A. Symbols and Notations

A list of symbols frequently used in this work is shown in table I in the order in which they appear.

B. Dynamic Window Approach

The Dynamic Window Approach (DWA) [4] mainly uses the following two stages to search for a collision-free, and reachable $[v, \omega]$ velocity vector in a 2-dimensional velocity space known as the dynamic window. The dynamic window is a discrete space with k^2 number of $[v, \omega]$ velocity vectors, where k is the number of linear and angular velocities that the robot can execute at any time instant.

1) *Search Space*: The goal of the first stage is to generate a space of reachable velocities for the robot. This stage involves the following steps.

Velocity Vectors Generation: In this step, according to the maximum linear and angular velocities the robot can attain, a set V of $[v, \omega]$ vectors is generated. Each velocity vector in the set corresponds to an arc of different radius that the robot can move along. The equations describing the trajectory of the robot for different $[v, \omega]$ vectors can be found in [4].

Admissible Velocities: After forming set V , for each $[v, \omega] \in V$, the distance to the nearest obstacle from its corresponding arc is computed. The $[v, \omega]$ vector is considered *admissible* only if the robot is able to stop before it collides

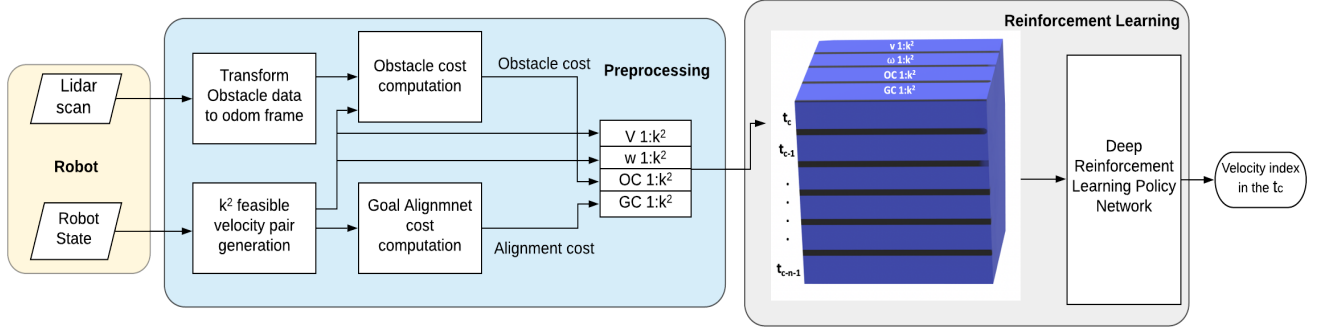


Fig. 2: (a) Shows the flow of our novel approach including the pre-processing step and the reinforcement learning part.

with the obstacle. The admissible velocity set V_{ad} is given by,

$$V_{ad} = \{v, \omega\} \quad \begin{aligned} v &\leq \sqrt{2 \cdot \text{dist}(v, \omega) \cdot \dot{v}_b}, \\ \omega &\leq \sqrt{2 \cdot \text{dist}(v, \omega) \cdot \dot{\omega}_b} \end{aligned} \quad (1)$$

$\text{dist}(v, \omega)$, is the distance to the nearest obstacle on the arc.

Dynamic Window: The next step is to further prune the set V_{ad} to remove the velocities that are not achievable within a Δt considering the robot's linear and angular acceleration limits. This final set is called the dynamic window and is formulated as.

$$V_d = \{v, \omega | v \in [v_a - \dot{v} \cdot \Delta t, v_a + \dot{v} \cdot \Delta t], \omega \in [\omega_a - \dot{\omega} \cdot \Delta t, \omega_a + \dot{\omega} \cdot \Delta t]\}. \quad (2)$$

2) *Objective Function Optimization:* In the second stage, the $[v, \omega]$ which maximizes the objective function defined in equation 3 is searched for in V_d .

$$G(v, \omega) = \sigma(\alpha \cdot \text{heading}(v, \omega) + \beta \cdot \text{dist}(v, \omega) + \gamma \cdot \text{vel}(v, \omega)). \quad (3)$$

For a $[v, \omega]$ executed by the robot, $\text{heading}()$ measures the robot's progress towards the goal (more progress \Rightarrow higher value), $\text{dist}()$ measures the robot's distance from the nearest obstacles (more distance \Rightarrow higher value), and the $\text{vel}()$ function checks that $v \neq 0$. α, β and γ denote weighing constants that can be tuned by the user.

Obstacle information embedded in the velocity space is utilized to select the optimal velocity pair. The $[v, \omega]$ vector computed by DWA may be a local minima. However, this issue can be mitigated if the connectivity of free space to the goal is known.

C. DRL Policy Training

DRL-based collision avoidance policies are usually trained in simulated environments using a robot which uses the said policy to perform certain *actions* based on environmental *observations* to earn some *rewards*. The robot's actions are represented by the velocities that it can execute, and the set of all the robot's velocities is called its action space. The robot's observation consists of information regarding the robot's environment (such as the poses of obstacles), and the set of all observations that the robot can make is called its

observation space. The policy is encoded as a deep neural network whose weights are updated during training.

The robot's primary objective is to maximize a *reward function* by performing the actions which are rewarded and avoiding actions or behaviors which are penalized. A typical reward function involves terms to provide positive reward for desirable behaviors such as the robot moving towards and reaching its goal, and to provide negative reward when the robot exhibits undesirable behaviors such as colliding with obstacles. We train our DRL-based collision avoidance policy based on the reward function using a well-known method known as Proximal Policy Optimization (PPO) [21].

Post training, a collision free velocity \mathbf{v}^{DRL} at each time instant is sampled from a trained policy π_θ as:

$$\mathbf{v}^{DRL} \sim \pi_\theta(\mathbf{v}^t | \mathbf{o}^t), \quad (4)$$

where \mathbf{v}^t and \mathbf{o}^t are the velocity and the observation spaces at time t , respectively.

IV. OUR APPROACH

In this section, we explain the construction of our novel observation space, reward function and our network architecture.

A. Observation Space Generation

The manner in which data in the observation space is represented is crucial for the policy training's success, since an important component of policy training is correlating the observations with desired actions. An ideal observation space must balance sufficiently encoding data about the environment and maintaining a low dimensionality. A low dimensional observation space does not require a complicated network architecture to process it, which in turn leads to lower training times.

In our work, the observation space is constructed using the robot's current feasible velocities (equation 2) and the environment's state is embedded as a matrix of costs for using those velocities for the current and past $n-1$ time instants. The action space is a single $[v, \omega]$ vector that the robot must execute at the current time instant that is computed by our fully trained DRL policy considering the time evolution of the environment's state for n time instants. The steps used in the observation space construction are detailed below.

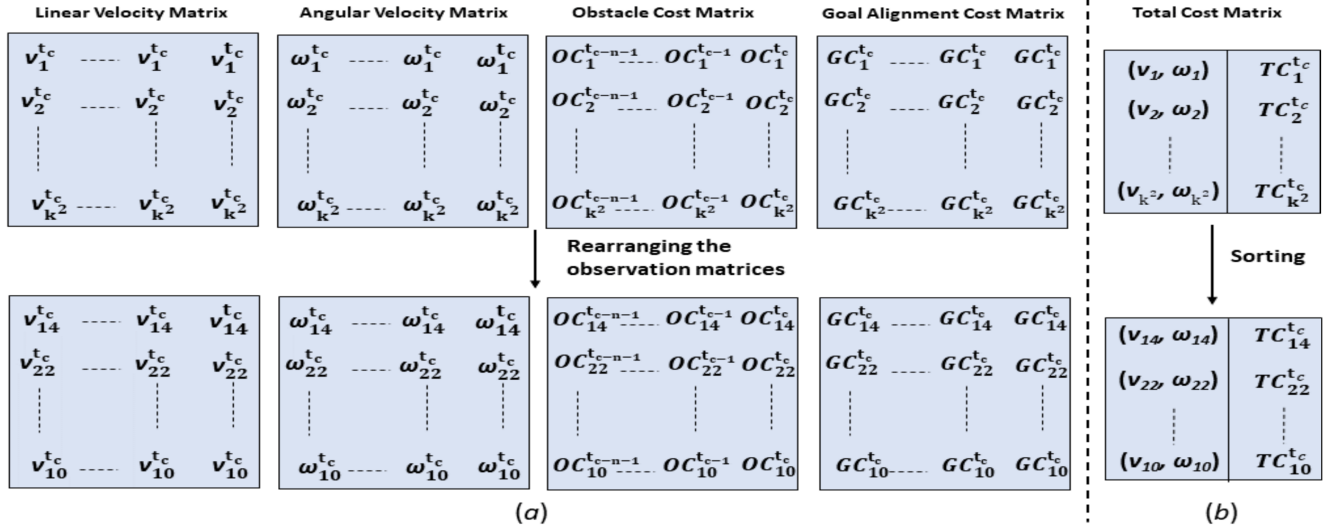


Fig. 3: (a)[Top] The initial construction of our observation space. Initially, the linear and angular velocity matrices ($[v, \omega] \in V_f$) along with their obstacle and goal alignment cost matrices for n time instants are constructed. [Bottom] The values in the four matrices are rearranged in the descending order of the total cost value at the current time instant. In this case shown, $[v_{14}, \omega_{14}]$ has the least total cost. (b)[Top] The total costs TC for each velocity vector belonging to set V_f . [Bottom] The velocity vectors rearranged in the descending order of the total cost at the current time instant.

1) *Dynamically Feasible Velocity Vectors*: Unlike DWA, we do not first generate an admissible velocity set V_{ad} that contains collision-free robot velocities. Instead, we first compute sets of feasible/reachable linear and angular velocities ($lin = [v_a - \dot{v} \cdot \Delta t, v_a + \dot{v} \cdot \Delta t]$ and $ang = [\omega_a - \dot{\omega} \cdot \Delta t, \omega_a + \dot{\omega} \cdot \Delta t]$) using equation 2. We discretize sets lin and ang into k intervals such that the total number of $[v, \omega]$ vectors obtained from the intervals is k^2 . We then form the set of feasible velocities V_f from these discretized sets as,

$$V_f = \{(v, \omega) | v \in lin_k, \omega \in ang_k\}. \quad (5)$$

The velocity vectors in V_f do not account for the locations of the obstacles in the current time instant t_c or the past $n-1$ time instants. Therefore some velocities in V_f could lead to collisions. The velocity vectors in V_f are appended $n-1$ times as column vectors in two matrices of size $(k^2 \times n)$ and the generated linear and angular velocity matrices are shown in the Fig. 3(a)[top].

2) *Obstacle sets*: We use the lidar scan to get the location of the obstacles around the robot. For each time instant, the obstacle locations are obtained relative to the fixed odometry frame of the robot and stored in a set. The odometry frame is attached to the ground at the location from which the robot started (see 4). Consider Fig. 4(a), the locations of two obstacles in the current as well as in the past $n-1$ time steps are shown. We add the set of obstacle locations in a list \mathcal{O} of length n (see Fig. 4(b)), where each column shows the set of obstacle locations for a specific time instant. We use list \mathcal{O} to incorporate the information of the motion of various obstacles in the environment.

3) *Obstacle cost calculation*: We next calculate the *obstacle cost* similar to the $dist()$ function used in equation 3 for every velocity vector in V_f . Each vector in V_f is forward simulated for a time Δt to check if it leads to a collision, given the obstacle positions in \mathcal{O} . The velocity vectors that lead to a collision are given higher costs and the velocities that are collision-free are assigned cost inversely proportional

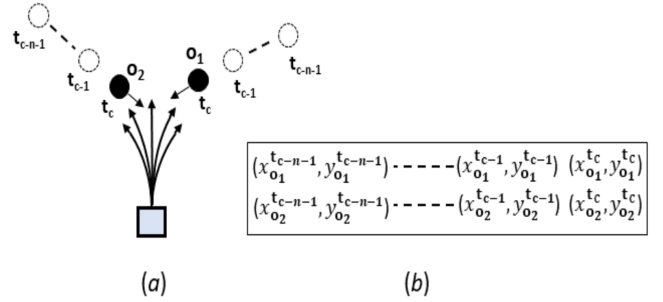


Fig. 4: Description of the obstacle set construction. (a) Shows the change in the location of the obstacle in the past $n-1$ time instances with respect to the location of the robot in the current time instance. (b) Shows the list of the obstacle sets obtained at various time instances

to the least distance of the obstacle from the arc generated after executing the velocity vector.

$$OC_i^{t_j} = \begin{cases} 40 & \text{if } dist^{t_j}(v_i, \omega_i) < R^{rob}, \\ \frac{1}{dist(v_i, \omega_i)} & \text{otherwise} \end{cases} \quad (6)$$

The Fig.3(a)[top] shows the obtained $(k^2 \times n)$ matrix of the obstacle costs.

4) *Goal alignment cost calculation*: Each $[v, \omega] \in V_f$ is forward simulated for a time Δt and the distance from the robot and its goal is measured. The velocity vectors that reduce the distance between the robot and the goal location are given a low cost. The goal alignment cost is independent of the location of the obstacles around the robot, therefore the same cost for each pair is appended for n times to obtain a goal alignment cost matrix of shape $(k^2 \times n)$ as seen in Fig. 3(a)[top].

$$GC_i^{t_c} = ||EndPoint(v_i, \omega_i) - \mathbf{g}|| * r_{ga} \quad (7)$$

Here, $EndPoint(v_i, \omega_i)$ function gives the coordinates of the end point of the trajectory generated by executing the

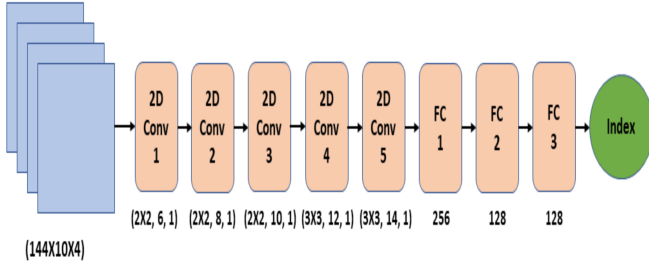


Fig. 5: Architecture of the policy network. The input is marked in blue, the network layers are marked in orange. The initial 5 layers are the convolutional layers and the remaining 3 layers are the fully connected layers. The output of the network is marked in green.

velocity vector (v_i, ω_i) and r_{ga} is a constant, we set $r_{ga} = 2.5$.

5) *Total cost calculation*: The total cost for the robot using a vector $[v_i, \omega_i]$ for the current time instant t_c is calculated as,

$$TC_i = OC_i^{t_c} + GC_i^{t_c} \quad (8)$$

and is shown in Fig.3(b)[top].

B. Pre-Processing

The linear, angular, obstacle cost and goal alignment cost matrices obtained previously are now pre-processed to better represent which velocities in V_f had the least costs given the obstacle positions for the past n time instants.

1) *Sorting the velocity vectors*: The velocity vectors are sorted in the descending order according to the total cost of the velocity vectors at the current time instant. The sorting step is shown in the Fig. 3(b). The elements in the linear, angular velocities, obstacle costs and goal alignment cost matrices are then rearranged in a similar manner (Fig.3(a)[bottom]).

2) *Observation space*: Finally, the pre-processed linear and angular matrices along with their obstacle as well as the goal alignment cost matrices are stacked up to get a matrix of size $(k^2 \times n \times 4)$, which is then passed to the policy network (see Fig.2).

C. Network Architecture

The policy network architecture used in this hybrid local planner is shown in Fig.5. Five 2-D convolutional layers, followed by 3 fully connected layers are used for processing the observation space. ReLU activation is applied to the output of the hidden layers before it is mapped to the action space vector \mathbf{v}^t . This action space vector holds the index of the ordered velocity pairs of the current time frame. This architecture is much simpler and requires fewer layers for handling our observation space.

D. Reward Shaping

The primary aim of the policy being trained is to reach the goal while steering clear of static and dynamic obstacles while enabling smooth navigation. Rewards for the basic navigation task of reaching the target and collision against obstacles are provided with higher positive or negative rewards correspondingly.

In order to enable faster convergence, the difference of distance from the goal in previous time step and current time instant is utilized. This incentivizes the policy to move the robot closer to goal every time step or get penalized as,

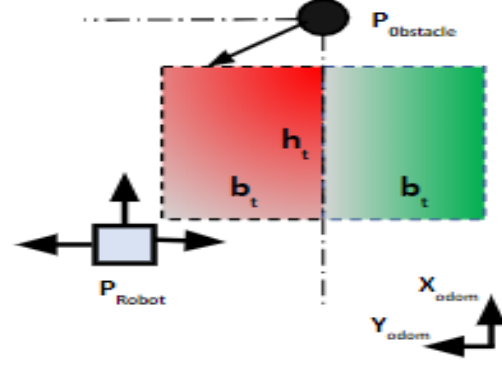


Fig. 6: Figure showing the reward values assigned during training when the robot encounters a dynamic obstacle. The trajectories leading the robot to the red region are penalized proportional to the intensity of the red color in that region. The trajectories leading to the green regions are rewarded.

$$(r_g)^t = \begin{cases} r_{goal} & \text{if } \|\mathbf{p}^t - \mathbf{g}\| < 0.3 \text{ meters,} \\ 2.5(\|\mathbf{p}^{t-1} - \mathbf{g}\| - \|\mathbf{p}^t - \mathbf{g}\|) & \text{otherwise.} \end{cases} \quad (9)$$

At any time instant t , the collision penalty is defined as,

$$(r_c)^t = \begin{cases} r_{collision} & \text{if } \|\mathbf{p}^t - \mathbf{p}_{obstacle}\| < 0.5 \text{ meters,} \\ 0 & \text{otherwise.} \end{cases} \quad (10)$$

When a dynamic obstacle (located at (x^{obs}, y^{obs})) is in the sweep radius of the robot (located at (x^{rob}, y^{rob})) relative to the odometry frame, we define the following parameters,

$$d_t = \text{dist}([x^{rob}, y^{rob}], [x^{obs}, y^{obs}]) \quad (11)$$

$$b_t = y^{rob} - y^{obs} \quad | \quad h_t = x^{rob} - x^{obs} \quad (12)$$

Since the policy must be capable of operating even in dense human crowds, if it computes a trajectory in the same relative direction as a dynamic obstacle (say a pedestrian), it increases the chance of collision. Trajectories that steer the robot to be on opposite side of a dynamic obstacle's heading direction (behind the obstacle) are therefore rewarded positively and all other trajectories are penalized based on the proximity to the obstacle (see Fig.6). This reward/penalty is denoted as,

$$(r_{steer})^t = \begin{cases} \frac{r_{proximal}}{d_t} - b_t * r_{heading} & \text{if } d_t < 3 \text{ \& } b_t > 0 \\ b_t * r_{heading} & \text{if } d_t < 3 \text{ \& } b_t < 0 \end{cases} \quad (13)$$

In case of a obstacle moving head-on, b_t is zero and total steering reward is zero. In the presence of multiple dynamic obstacles proximal to the robot, the union of the red zones as shown in the figure is negatively rewarded.

This is also supplemented by providing negative rewards inversely proportional to distance from obstacles near the robot. This reduces the danger of collision as negative reward is accumulated as the robot approaches the obstacle.

$$(r_{dangerOfCollision})^t = \frac{r_{dCollision}}{d_t} \quad (14)$$

We set $r_{goal} = 2000, r_{collision} = -2000, r_{proximal} = -10, r_{heading} = 25, r_{dCollision} = -3$.

V. RESULTS AND EVALUATIONS

A. Implementation

We train the deep reinforcement learning policy in a simulator and test the trained models in the simulation as well as on the real robot. We use ROS Melodic and Gazebo 9 to create the simulation environments on a workstation with an IntelXeon 3.6GHz processor and an Nvidia GeForce RTX 2080TiGPU. We implement the policy network using tensorflow and use the PPO2 implementation provided by stable baselines to train the policy. We simulate multiple copies of Turtlebot 2 model with a Hokuyo Lidar in parallel to train the models in the simulation. The different copies of Turtlebot 2 are deployed in different scenarios of the same simulation environment, this makes sure that the model does not over fit to a particular scenario.

B. Testing Scenarios

We test the performance of our approach and the prior approaches in different high fidelity simulation environments. The simulation environments that we use, characterize the pedestrian robot interactions in the different indoor and outdoor scenarios. We assume that the robot is taking the full responsibility of the collisions. We evaluate our method and the prior approaches in the following test environments, **Zigzag static**: This scenario contains many turns with number of static obstacles. This scenario tests the performance of various approaches in densely cluttered static environment.

Occluded-Ped: Scenario with many turn and pedestrians that are occluded by the walls. Using this scenario, we test the how different approaches handle the obstacles when they are suddenly introduced in the sensor's field of view.

Sparse dynamic environment: Scenario contains sparse dynamic pedestrians, the environment contains 4 pedestrians. The pedestrians are walking at 45° and 90° with the line connecting the robot's start and goal locations. This scenario mainly evaluate the robot's ability to handle dynamic obstacles and plan a path that doesn't lead to collision.

Dense dynamic environment: This scenario has a total of 16 pedestrians. It contains both static and dynamic pedestrians. It tests the behaviour of various algorithm in the dense dynamic environments.

C. Evaluation Metrics

We compare our approach with two other classical and learning based collision avoidance techniques: (i) Dynamic Window Approach [4] (ii) Long et al. [18]. We also provide some ablation study results to show effects of various design choices that we made in our approach. We use the following metrics to compare the performance of various collision avoidance algorithms and the ablation study models. We use the following metrics to compare the performance of various collision avoidance algorithms.

- **Success Rate** - The number of times the robot reached the goal without colliding with the obstacles over 50 randomly initialized episodes.
- **Average Trajectory Length** - It is the total distance traversed by the robot, until the goal is reached, averaged over the number of successful attempts.
- **Average Velocity** - The average velocity of the robot is computed as the trajectory length over the time taken to reach the goal in a successful trial.

Metrics	Method	Sparse Dynamic Env.	Zigzag static	Occluded-Ped	Dense Dynamic Env.
Success Rate	Hybrid RL (Our Method)	0.54	1.0	1.0	0.4
	DRL	0.3342	1.0	.76	.31
	DWA	0.42	1.0	0.9	0.3
Avg Trajectory Length (m)	Hybrid RL (Our Method)	11.95	28.85	27.26	12.23
	DRL	12.1	26.89	25.63	11.57
	DWA	11.99	26.62	25.07	12.81
Avg Velocity (m/s)	Hybrid RL (Our Method)	.42	.38	.46	.37
	DRL	.37	.42	.51	.503
	DWA	.6	.435	.568	.64

TABLE II: Relative performance of our hybrid RL method versus learning based and classical local planners.

Metrics	Method	Sparse Dynamic Env.	Zigzag Static	Occluded-Ped	Dense Dynamic Env.
Success Rate	With positive reinforcement	0.54	1.0	1.0	.42
	Without positive reinforcement	.44	.86	.64	.4
Avg Trajectory Length	With positive reinforcement	11.95	28.85	27.26	12.46
	Without positive reinforcement	11.6	28.12	27.86	12.78
Avg Velocity	With positive reinforcement	.42	.37	.47	.38
	Without positive reinforcement	.41	.34	.41	.34

TABLE III: Ablation study showing relative performance of the models trained with positive reinforcement and without positive reinforcement.

D. Analysis and Comparison

The performance comparison of our method versus the prior approaches in various test environments is show in Table. II. The results of ablation study showing the benefits of adding positive reinforcement and 4 layer observation space are given in the Table. III and IV.

We present the comparison of our method with prior collision avoidance methods in Table. II. We can observe that in terms of success rate all the approaches perform well in the Zigzag static scenario. But when the number of dynamic obstacles increases in the environment we can clearly see our method performs better compared all other methods. The DWA approach does not consider the temporal information while navigating through the dynamic obstacles and this lead to collisions as the density of the dynamic obstacles increases in the environment. Whereas our approach uses the information of the past n time steps to make navigation decisions also formulation of the reward function helps the policy to handle dynamic obstacles better compared to other learning based approaches. In the Occluded Ped test scenario, the pedestrians are suddenly introduced in the field of view of the lidar sensor. The DWA and the DRL approach can not handle the occluded pedestrians well. However, our approach with limited temporal information can still perform better.

Ablation Study for the Positive Reinforcement We show the benefits of adding positive reinforcement for in the reward function. For the ablation study, we compare two models trained with and without positive reinforcement in different test environments. From the Table III, we can clearly see that the model that is trained with positive reinforcement out performs the model that is trained without positive reinforcement in all the test environments.

Ablation Study for the Observation Space We use the observation space of 4 different matrices as show in Fig. 3. The observation space includes a linear velocity frame, angular velocity frame, obstacle cost frame and goal alignment cost. We compare this formulation of the observation space with a 3 frame observation space where we use a linear velocity frame, angular velocity frame and total cost frame. We hypothesis that the 4 frame observation space can better impart the information about the obstacles around the robot as the obstacle cost is provided separately whereas in the 3 layer observation space the obstacle cost is added in the goal alignment cost to obtain the total cost. For this ablation study, we train models with a 3 frame and 4 frame observation space, we keep all other parameters the same for both of the models. The results for both the models are shown in Table

Metrics	Method	Sparse Dynamic Env.	Zigzag static	Occluded-Ped	Dense Dynamic Env.
Success Rate	3 layer	.36	.82	.94	.36
	4 layer	0.54	1.0	1.0	.42
Avg Trajectory Length	3 layer	11.56	27.93	27.04	12.34
	4 layer	11.95	28.85	27.26	12.46
Avg Velocity	3 layer	.46	.38	.44	.37
	4 layer	.42	.37	.47	.38

TABLE IV: Ablation study showing relative performance of the models trained with total cost observation space and individual cost observation space.

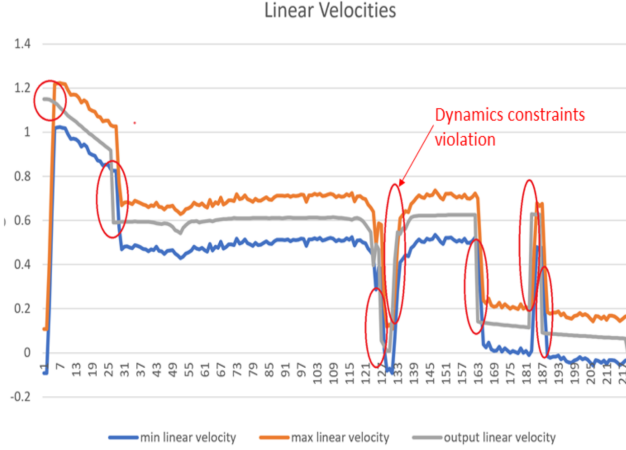


Fig. 7: Graph showing the change in the linear velocity generated by the DRL approach along with the maximum and the minimum achievable velocity at that time instance.

IV. We can observe that the 4 frame model performs better compared to the 3 frame model in all of the test scenarios.

Dynamics Constraints Violation We measure the number of dynamics constraints violations by our approach and the learning based collision avoidance techniques. The Fig. 7 shows the graph of linear velocities generated by the DRL approach in the Sparse Dynamic environment. The red circles marked on the figure shows the time steps at which the method violated the dynamics constraints. We observed when the robot starts from the initial location or when the robot stops to avoid the collision it most of the time chose the velocities that were not in the dynamically feasible velocity space. In the complete trajectory from the start to the goal location, the DRL method violated the dynamics constraints for 10 % of the total time steps.

VI. CONCLUSIONS, LIMITATIONS AND FUTURE WORK

We present a novel formulation of the deep reinforcement learning policy that generates dynamically feasible and spatially aware smooth velocities. Our method rectifies the issues associated with the learning based approaches and the classical Dynamic Window Approach. We validate our approach in the simulation and in the real world environments. We compare our approach with the other collision avoidance techniques in terms of the collision rate, average trajectory length, average velocity and dynamically feasible velocity vector generation. We also implement our approach on two differential drive robots: Clearpath Turtlebot2 and Jackal, and show the performance improvements in the real world. Our work has several limitations as well. The model uses the information of past few seconds to make decision, if any obstacle is suddenly introduced in the field of view of the robot then the policy might not have enough information to make informed decisions and the robot might freeze. The current model uses convolutional neural network as the

policy network, but in future we would like to train a model based on LSTM [22] policy and we would also like to modify the reward function to get better navigation behavior.

REFERENCES

- [1] P. Trautman, J. Ma, R. M. Murray, and A. Krause, "Robot navigation in dense human crowds: Statistical models and experimental studies of human-robot cooperation," *The International Journal of Robotics Research*, vol. 34, no. 3, pp. 335–356, 2015. [Online]. Available: <https://doi.org/10.1177/0278364914557874>
- [2] J. Liang, U. Patel, A. Sathiamoorthy, and D. Manocha, "Crowd-steer: Realtime smooth and collision-free robot navigation in densely crowded scenarios trained using high-fidelity simulation," 07 2020, pp. 4193–4200.
- [3] M. Everett, Y. F. Chen, and J. P. How, "Collision avoidance in pedestrian-rich environments with deep reinforcement learning," 2019.
- [4] D. Fox, W. Burgard, and S. Thrun, "The dynamic window approach to collision avoidance," *IEEE Robotics Automation Magazine*, vol. 4, no. 1, pp. 23–33, 1997.
- [5] T. Fan, P. Long, W. Liu, and J. Pan, "Fully distributed multi-robot collision avoidance via deep reinforcement learning for safe and efficient navigation in complex scenarios," *CoRR*, vol. abs/1808.03841, 2018. [Online]. Available: <http://arxiv.org/abs/1808.03841>
- [6] A. J. Sathiamoorthy, J. Liang, U. Patel, T. Guan, R. Chandra, and D. Manocha, "Denseavoid: Real-time navigation in dense crowds using anticipatory behaviors," 2020.
- [7] E. W. Dijkstra, "A note on two problems in connexion with graphs," *Numerische mathematik*, vol. 1, no. 1, pp. 269–271, 1959.
- [8] P. Hart, N. Nilsson, and B. Raphael, "A formal basis for the heuristic determination of minimum cost paths," *IEEE Transactions on Systems Science and Cybernetics*, vol. 4, no. 2, pp. 100–107, 1968. [Online]. Available: <https://doi.org/10.1109/tssc.1968.300136>
- [9] S. M. Lavalle, "Rapidly-exploring random trees: A new tool for path planning," Tech. Rep., 1998.
- [10] S. Karaman, M. R. Walter, A. Perez, E. Frazzoli, and S. Teller, "Anytime motion planning using the rrt*," in *2011 IEEE International Conference on Robotics and Automation*, 2011, pp. 1478–1483.
- [11] R. Simmons, "The curvature-velocity method for local obstacle avoidance," in *Proceedings of IEEE International Conference on Robotics and Automation*, vol. 4, April 1996, pp. 3375–3382 vol.4.
- [12] C.-C. Chou, F.-L. Lian, and C.-C. Wang, "Characterizing indoor environment for robot navigation using velocity space approach with region analysis and look-ahead verification," *Instrumentation and Measurement, IEEE Transactions on*, vol. 60, pp. 442 – 451, 03 2011.
- [13] E. J. Molinos, Ángel Llamazares, and M. Ocaña, "Dynamic window based approaches for avoiding obstacles in moving," *Robotics and Autonomous Systems*, vol. 118, pp. 112 – 130, 2019. [Online]. Available: <http://www.sciencedirect.com/science/article/pii/S0921889018309746>
- [14] D. Fox, W. Burgard, S. Thrun, and A. B. Cremers, "A hybrid collision avoidance method for mobile robots," in *Proceedings. 1998 IEEE International Conference on Robotics and Automation (Cat. No.98CH36146)*, vol. 2, May 1998, pp. 1238–1243 vol.2.
- [15] L. Xie, S. Wang, A. Markham, and N. Trigoni, "Towards monocular vision based obstacle avoidance through deep reinforcement learning," *CoRR*, vol. abs/1706.09829, 2017. [Online]. Available: <http://arxiv.org/abs/1706.09829>
- [16] Y. Kim, J. Jang, and S. Yun, "End-to-end deep learning for autonomous navigation of mobile robot," in *2018 IEEE International Conference on Consumer Electronics (ICCE)*, Jan 2018, pp. 1–6.
- [17] B. Lütjens, M. Everett, and J. P. How, "Safe reinforcement learning with model uncertainty estimates," in *2019 International Conference on Robotics and Automation (ICRA)*, May 2019, pp. 8662–8668.
- [18] P. Long, T. Fan, X. Liao, W. Liu, H. Zhang, and J. Pan, "Towards optimally decentralized multi-robot collision avoidance via deep reinforcement learning," in *2018 IEEE International Conference on Robotics and Automation (ICRA)*, May 2018, pp. 6252–6259.
- [19] M. Everett, Y. F. Chen, and J. P. How, "Motion planning among dynamic, decision-making agents with deep reinforcement learning," in *2018 IEEE/RSJ International Conference on Intelligent Robots and Systems (IROS)*, Oct 2018, pp. 3052–3059.
- [20] L. Tai, J. Zhang, M. Liu, and W. Burgard, "Socially compliant navigation through raw depth inputs with generative adversarial imitation learning," in *ICRA*, May 2018, pp. 1111–1117.
- [21] J. Schulman, F. Wolski, P. Dhariwal, A. Radford, and O. Klimov, "Proximal policy optimization algorithms," 2017.
- [22] S. Hochreiter and J. Schmidhuber, "Long short-term memory," *Neural Comput.*, vol. 9, no. 8, p. 1735–1780, Nov. 1997. [Online]. Available: <https://doi.org/10.1162/neco.1997.9.8.1735>